J. COMBIN. MATH. COMBIN. COMPUT. 127b (2025) 8723--8745

Journal of Combinatorial Mathematics
and Combinatorial Computing
www.combinatorialpress.com/jcmcc

Machine Learning-Based State Monitoring and Regulation Characterization of Distribution Grid with High Percentage Distributed Resource Access

Yixin Xia[1], Zhongqiang Zhou[2,✉], Yuan Wen[3], Jun Ao[4], Ying Lu[5], Jingrong Meng[6]

[1] *Bijie Power Supply Bureau, Guizhou Power Grid Dispatching Control Center, Bijie, Guizhou, 551700, China*
[2] *Automation Department, Guizhou Power Grid Dispatching Control Center, Guiyang, Guizhou, 550000, China*
[3] *Kaili Power Supply Bureau, Guizhou Power Grid Dispatching Control Center, Kaili, Guizhou, 556000, China*
[4] *Automation Division, Guiyang Power Supply Bureau Dispatching Control Center, Guiyang, Guizhou, 550000, China*
[5] *Zunyi Power Supply Bureau, Guizhou Power Grid Dispatching Control Center, Zunyi, Guizhou, 563000, China*
[6] *Center for New Power Systems and Artificial Intelligence, Sichuan Research Institute, Shanghai Jiao Tong University, Chengdu, Sichuan, 610213, China*

ABSTRACT
The large number of accesses of distributed power supplies changes the distribution network from a passive network to an active network with small and medium-sized power supplies all over the network, which brings important impacts on all aspects of the distribution network, such as planning, operation, and power quality. The study analyzes the types of distributed power nodes and the traditional trend model of distribution network, studies the changes of voltage and network loss after the integration of distributed power sources into the distribution network, and analyzes the impact of different numbers, capacities and access locations of distributed power sources on the reactive power optimization of the distribution network by means of IEEE33 nodes. Analyze the impact of distributed power supply on distribution network. Firstly, the characteristics of distributed power supply are analyzed, distributed photovoltaic and distributed wind power operation models are established, and the influencing factors of the two power supply outputs are analyzed to generalize the distributed power supply output model. The basic principle of weighted least squares state estimation and its algorithmic process are introduced, and on its basis, an equation-containing constrained state estimation model for dealing with zero-injection nodes in the distribution network is introduced, and finally, the feasibility and validity of the proposed constrained state estimation model's state estimation method for the distribution network are verified through the analysis of an example of the IEEE 33-node system. Combining the sequence quadratic programming method and the idea of trust domain, the trust domain sequence quadratic programming method is proposed, and the use of the effective set method to quickly solve the subquadratic programming problem after downsizing is the key that the algorithm in this paper can solve the optimization problem relatively quickly. The

✉ Corresponding author.
E-mail address: gzdwzzq@163.com (Z. Zhou).
Received 12 January 2024; Revised 25 March 2024; Accepted 25 December 2024; Published Online 16 April 2025.
DOI: 10.61091/jcmcc127b-479

optimization results show that distributed power sources participate in active distribution network reactive power optimization and cooperative control to provide a theoretical basis, and the effectiveness of the method is verified through simulation cases.

Keywords: distribution network, distributed power supply, basic weighted least squares, cooperative control

1. Introduction

With the continuous development of social productivity, the maintenance of electric power equipment with the development of science and technology from the original aftermath maintenance, gradually developed to preventive maintenance, and is constantly accelerating to the state maintenance stage. By carrying out condition monitoring to realize when the repair is repaired, so as to avoid excessive repair and when the repair is not repaired, in order to further improve the reliability and safety of power equipment operation [1-4]. The core meaning of the word "when" is to accurately determine the state of the equipment in real time to the extent that it needs to be "repaired". In a nutshell, condition monitoring is online or offline can directly or indirectly, intuitively or implicitly reflect and characterize the operating state of the equipment signal sensing, acquisition, transmission, processing, preliminary diagnosis and other series of detection and monitoring methods, means, technology and devices [5-8]. Fault diagnosis is a manual or production operation system to analyze and judge the parameters, issue fault repair instructions and carry out maintenance work. Although from the technical point of view, the traditional preventive test of electric power equipment and its institutional arrangement can judge the equipment status to a certain extent, but from the real-time point of view and accuracy point of view, the preventive test is not enough to fully support the diagnostic level required for condition maintenance [9-12]. Therefore, the realization of condition perception through condition monitoring becomes an inevitable choice and development trend. With the promotion and implementation of development plans such as China's smart grid and ubiquitous power Internet of Things, the connotation of condition maintenance becomes more and more rich and far-reaching [13-16]. Conditional maintenance compared to preventive maintenance, can realize the number of power outages and the number of operations of the double decline, improve equipment utilization and service life. At the same time, the innovation and development of condition maintenance in technology will lead to the optimization of the internal management process and mechanism of electric power enterprises, from the traditional more dispersed maintenance mode, transformed into a new mode of systematic comprehensive judgment, multi-professional departments collaborate with each other [17-20]. Therefore, the study of machine learning-based state monitoring and regulation characteristics of distribution network with high percentage of distributed resources accessing the distribution network will help to monitor the state of the distribution network online and offline, and provide relevant monitoring data for the auxiliary decision-making system of the distribution network state maintenance, which will make the degree of automation of the distribution network state maintenance greatly improved [21-24].

This paper describes the relationship between distributed power sources and distribution network by describing the relationship between distributed power sources and distribution network. The IEEE 33-node system is used to analyze the impact of different numbers, capacities and grid-connected locations of distributed power sources on the reactive power optimization of distribution grids, and then the operational indicators affecting the safe operation of distribution grids are analyzed from the perspective of the physical model, including the static voltage stability indicator, the indicator of the rate of change of the system network loss, and the fluctuation range of each indicator is calculated. On the basis of weighted least squares state estimation, an equation-containing constrained state estimation model for dealing with zero-injection nodes in the distribution network is introduced, and the feasibility and validity of the proposed constrained state estimation model's state estimation method for the distribution network is verified through the analysis of the IEEE 33-node system example, and finally, the branch delimitation method is used with the quadratic programming algorithm of the sequence of the reliance domain to find the solution.

2. Analysis of the impact of a high percentage of distributed resources on the distribution grid

2.1. Distribution network current calculation model with high percentage of DGs

2.1.1. Distributed Power Tide Modeling. Renewable energy generation equipment itself has an impact on the distribution network trend operation, which is generally categorized into three types of PQ nodes, PV nodes and balancing nodes, of which PQ nodes are mostly load nodes; balancing nodes are mostly power nodes, and PV nodes appear less often. Due to the different types of renewable energy power generation equipment accessing the nodes, which in turn leads to changes in the types of distribution network nodes, combined with the existing research, the trend model of renewable energy power generation equipment itself can be divided into four categories: PQ-type, PV-type, PI-type, and PQ(V)-type. Among them, PQ-type and PV-type are the same as the traditional distribution network trend node types, and PI-type and PQ(V)-type are node types not found in the traditional distribution network.

1) PQ constant type distributed power model. After renewable energy power generation is connected to the distribution network, the renewable energy generation power is in the opposite direction to the load power, which can be understood as the load with negative renewable energy generation power. This type is mostly wind power generation, such as asynchronous generator wind turbine is treated as a negative load, access to the grid model is as follows:

$$\begin{cases} P = -P_s \\ Q = Q_s \end{cases} \tag{1}$$

where: P_s is active power, Q_s is reactive power.

2) PV Constant Distributed Power Modeling. The PV node can be used as a load node, which is characterized by the node voltage magnitude remains constant, if the node belongs to the PV node, it represents that the node output is continuously injected with the appropriate reactive power to vet the node voltage magnitude constant. The access to the grid is modeled as follows:

$$\begin{cases} P = -P_s \\ U = U_s \end{cases} \tag{2}$$

where: U_S is the voltage of the distributed power supply.

3) PI constant distributed power model. The PI node can be used as a load node, the active power and current magnitude of this node are maintained constant, and the access to the grid is modeled as follows:

$$\begin{cases} P = -P_s \\ I = I_s \end{cases} \tag{3}$$

where: I_S is the current of the distributed power supply.

The PI node output reactive power is:

$$Q_{k+1} = -\sqrt{|I|^2 (e_k^2 + f_k^2) - P^2} \tag{4}$$

where: e_k is the real part of the voltage; f_k is the imaginary part of the voltage; I is the current magnitude.

4) PQ(V) Constant Distributed Power Modeling. PQ (V) node can be used as a load node, generally appearing in the renewable energy generation access to the distribution network, such nodes involve more parameters, the calculation is more complex, the general way of dealing with the following: renewable energy power generation is mainly based on wind power generation, wind generators to asynchronous generators are predominantly used to calculate the reactive power consumed by the wind generator in the process of operation, generally using the method of shunt capacitors to determine. The access grid model is as follows:

$$\begin{cases} P = -P_s \\ Q_{k+1} = -f(U_k) \end{cases} \tag{5}$$

In addition, under certain conditions, a PQ(V) node can be converted to a PQ node, provided that the number of shunt capacitor inputs is greater than the maximum number that can be input.

2.1.2. Distribution network current calculation with DG. The traditional distribution network has only one power source, and the current is transmitted in a single direction along the power source-load, and the access of distributed power sources changes the characteristics of this single-direction transmission of the current, which is related to the access location and capacity of distributed power sources, and makes the distribution network node voltage, network loss and other parameters change.

Distribution network trend calculation (including traditional trend calculation and optimal trend calculation) is the basis for analyzing the distribution network node voltage, network loss, branch overload, the traditional general use of the Newton-Raphson method, Gaussian Saidel method of distribution network trend calculation, but due to the traditional distribution network trend calculation method will be due to the access of distributed power to change the direction of the trend is no longer applicable [25]. In order to solve this problem, scholars have proposed the branch method and node method to calculate the distribution network trend of multiple power supply access, and the difference between traditional algorithms lies in the selection of variables, the branch method to establish the system state equation and solve it with the parameters of the distribution system branch (power or current), including the method of forward back to the generation method and loop impedance method; the node method selects the node's injected current or power as well as the node voltage as the object of the study, and typical node methods are Newton method Typical nodal methods include Newton's method and various kinds of fast decoupling algorithms.

The above methods can be applied to the distribution network trend optimization of distributed power access, but for the distribution network with more nodes, there are more variables, more nonlinear equations and other problems, which directly lead to the distribution network trend calculation time is too long. For this reason, this paper adopts the second-order cone relaxation planning method to reduce the number of nonlinear equations and nonlinear variables, and at the same time, the method can be compatible with the CPLEX solver to solve, which effectively reduces the time and improves the quality of solution for distributed power supply access to distribution network currents.

2.2. Impact of high percentage of DG on distribution network operation

2.2.1. Impact of DG on distribution network currents. The topology of the distribution network presents a radial type, and the distribution network current flows from the energy side to the load side, and with the flow of the current, the grid voltage magnitude decreases along the direction of the current due to the network losses caused by the resistance and reactance of the distribution network. When renewable energy power generation is connected to the grid, it makes the voltage at the renewable energy access point increase, and if the renewable energy power generation equipment access is more, or the access capacity is larger, or the load at that node is smaller, it will lead to the load node voltage being higher than the substation bus voltage, which results in the distribution network trend flowing in the reverse direction, and increases the uncertainty and difficulty of the optimal tidal current calculation of the distribution network [26].

2.2.2. Impact of DG on distribution network voltage. When the distributed power supply accesses the distribution network, according to the different access position and access capacity, the distribution network voltage distribution exists as follows:

1) When the distributed power supply capacity is small and accesses the end load position, the distribution network end load voltage is raised by a small margin, but due to the small access capacity, the distribution network network overall tidal current distribution law basically remains unchanged, and the voltage is gradually lowered from the first end node to the end node.

2) When the distributed power supply capacity is larger and accesses the end load position, the end load voltage of the distribution network is greatly improved, and when the capacity of distributed power supply is larger than the load power of the access point, the voltage at the end of the line is higher than that at the first end of the line, and there is a bi-directional trend in the distribution network, and the voltage distribution of the distribution network is changed.

3) When the distributed power supply capacity is larger and access balance node, at this time, although the access distributed power supply capacity is larger, it will not change the direction of distribution network trend distribution, the distribution network trend is still flowing from the first end to the end, and from the first end to the end, the voltage still presents a gradual reduction trend.

2.3. Example analysis

2.3.1. Static voltage stability indicators. The simulation process of the static voltage stability index by connecting the distributed power supply in Table 1 to the distribution system is as follows:

1) Find the system branch impedance matrix Z.

2) Calculate the system node voltage value U_i, active P_i and reactive Q_i.

3) Operate the static voltage stability index $\alpha_i j$ for branch ij.

4) Find the maximum value of system static voltage stability index $\alpha_{\max}$.

5) Change the penetration rate of distributed power in the access system and repeat the above steps.

Table 1. Basic parameters of distributed power supply simulation

Distributed power number	Access node	Node type	P_{DG}/p.u	Q_{DG}/p.u	Node voltage
DG1	2	PV	0.007	-	1.01
DG2	5	PQ	0.007	0.005	-
DG3	11	PQ	0.007	0.007	-
DG4	28	PQ	0.007	0.007	-

Distributed power penetration is set to 0, 20%, 40%, 60%, 80% and 150%, and the results of a_{max} operation are shown in Table 2.

Table 2. Static voltage stability index

Permeability	0	20%	40%	60%	80%	150%
a_{max}	1.1431	0.1354	0.1276	0.1157	0.1396	0.1538

The voltage at each node for different permeability is shown in Fig. 1. The static voltage stability index of each branch is shown in Figure 2. As can be seen from Figure 1, after the access of distributed power supply, the system node voltage gets a significant increase in the level. With the increase of distributed power supply access capacity node voltage level continues to improve, the overall trend after accessing different penetration rates is similar to the trend when not accessing distributed power supply. At the same time, it can be seen from Figure 2, after increasing the penetration rate of distributed power supply, the system of static voltage stability indicators of each branch circuit continues to decline, the voltage stability of the corresponding enhancement, and stability to improve the stronger points are distributed power supply access nodes. It can be seen that different distributed power supply access penetration rate on the distribution network static voltage impact, the two nearly proportional relationship. Distributed power access in the branch with poor static stability, by increasing the static voltage of the corresponding branch, the static voltage stability of the distribution network is effectively improved.

Although distributed power supply access can provide a strong side to the distribution network voltage, but access to distributed power supply penetration is too large will make the system work at high voltage levels, access to distributed power supply access capacity of 150% of the load capacity of the system, there are multiple node voltage overruns in the system, affecting the normal operation of electrical equipment.

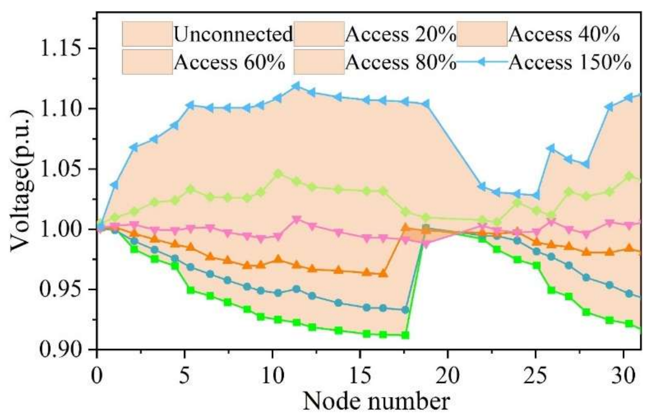

Fig. 1. Relationship between permeability and static voltage of DG

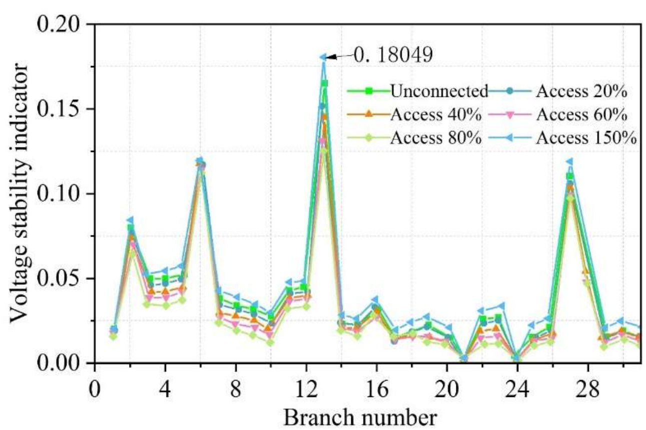

Fig. 2. Voltage stability index

2.3.2. Rate of change of network losses. When analyzing the rate of change of system network loss, the rate of change of system network loss is calculated from the consideration of two aspects: the access capacity of distributed power supply and the access location, respectively calculating the total network loss of the system without accessing distributed power supply and the total network loss of the system after accessing distributed power supply. The distributed power supply access program is:

1) Unchanged access location. Accessing DG3 alone and changing the DG3 injection power, the variation of the system network loss change rate β with the distributed power injection capacity is shown in Fig. 3. From the figure, it can be seen that with the increasing power injected by the distributed power supply, the change trend of the network loss change rate β is first increasing and then decreasing. It can be seen that the distributed power access capacity is not the larger the better, but there is an injection value that minimizes the system network loss value. When configuring the distributed power capacity, the system network loss is lower when the distributed power access capacity is 1400kW~2000kW.

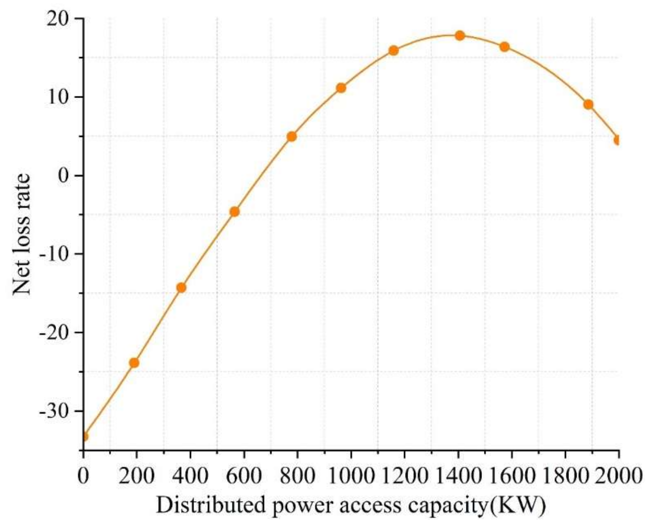

Fig. 3. Relationship between access capacity and network loss change rate

2) Constant access capacity. The distributed power supply with constant injected power of 800kW is connected to each node of the system respectively, and the rate of change of the system network loss β is shown in Fig. 4. From the figure, it can be seen that the distributed power supply access location on the total system network loss has a greater impact, access nodes 6-17, nodes 26-32 when the system network loss is small, connected to the 1, 18, 19, 20, 21 nodes when the system network loss is relatively large, so when configuring the distributed power supply in the distribution network, the consideration of the system's total network loss factors should be accessed in the middle of the line and the middle of the middle of the back position. In addition, the system network loss when connecting 4MW distributed power supply to 11 points and 1MW distributed power supply to 2, 5, 11 and 28 nodes respectively is 180.2kW and 96kW, from which it can be seen that the decentralized access to distributed power supply system network loss is lower compared to the centralized access.

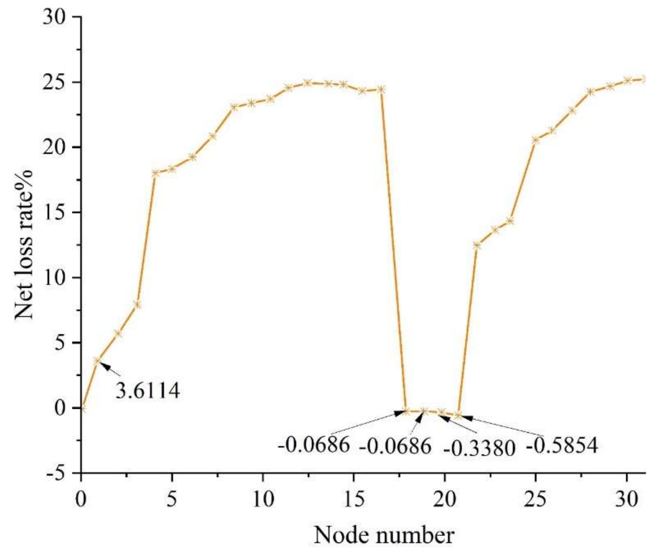

Fig. 4. Influence of access location on distribution network loss

3. State estimation of high percentage of DG access to the distribution network

3.1. Weighted least squares based state estimation model

As a classical algorithm for state estimation with good convergence and high estimation quality, the weighted least squares method is the most widely used, which is an estimation method that obtains the optimal solution of the state variables by finding the minimum value of the weighted least square sum of the measurement errors under the conditions of given network wiring, branch parameters, and measurement information [27].

3.1.1. Fundamentals of the algorithm. Given the network wiring, branch parameters, and quantity measurements, the system state variables and quantity measurements satisfy the following relationship:

$$z = h(x) + v \tag{6}$$

In the formula, $z = [z_1, z_2, \cdots, z_m]^{\mathrm{T}}$ represents the measurement phase, the number of measurement is m; $x = [x_1, x_2, \cdots, x_n]^{\mathrm{T}}$ represents the state variable phase, the number of state variables is n; $h(x) = [h_1(x), h_2(x), \cdots, h_m(x)]^{\mathrm{T}}$ represents the measurement function phase, whose dimension is the same as that of the measurement phase, which describes the nonlinear mathematical relationship between the measurement and the state variables; $v = [v_1, v_2, \cdots, v_m]^{\mathrm{r}}$ represents the m-dimensional measurement error phase.

The weighted least squares method is to obtain the optimal solution of the state variable by minimizing the weighted sum of squares of the measurement error, so the objective function can be established as:

$$\min J(x) = [z - h(x)]^{\hat{u}} W [z - h(x)] \tag{7}$$

where W denotes the $m \times m$ -dimensional measurement weight redown, $W = diag(1/\sigma_1^2 .1/\sigma_2^2, \cdots .1/\sigma_n^2)$ where σ_i denotes the ith measurement error standard deviation.

Since the measure function $h(x)$ is a nonlinear function of the state variable most x, it is not possible to compute the estimate of the state variable $\hat{x}$ in a self-adjoint manner, and it can be solved using the Newton Raphson iterative algorithm. Linearize $h(x)$: Let x_0 be some approximation of the state variable x, and Taylor expand $h(x)$ around x_0 to obtain an approximate linear expression for $h(x)$ after neglecting quadratic and higher nonlinear terms:

$$h(x) \approx h(x_0) + H(x_0)\Delta x \tag{8}$$

where $\Delta x = x - x_0$ denotes the correction of the state variable; $H(x)$ denotes the $m \times n$ th order Jacobi matrix consisting of the partial derivatives of the measurement function with respect to the state variable x, which is calculated by the formula:

$$H(x) = \frac{\partial h(x)}{\partial x} = \begin{bmatrix} \frac{\partial h_1(x)}{\partial x_1} & \frac{\partial h_1(x)}{\partial x_2} & \cdots & \frac{\partial h_1(x)}{\partial x_n} \\ \frac{\partial h_2(x)}{\partial x_1} & \frac{\partial h_2(x)}{\partial x_2} & \cdots & \frac{\partial h_2(x)}{\partial x_n} \\ \vdots & \vdots & \ddots & \vdots \\ \frac{\partial h_m(x)}{\partial x_1} & \frac{\partial h_m(x)}{\partial x_2} & \cdots & \frac{\partial h_m(x)}{\partial x_n} \end{bmatrix} \tag{9}$$

Bringing Eq. (8) into Eq. (7) yields the state estimation objective function under the linearized measure function:

$$\min J(x) = [\Delta z - H(x_0)\Delta x]^T W[\Delta z - H(x_0)\Delta x] \tag{10}$$

where $\Delta z = z - h(x_0)$ represents the amount of measurement error phase.

3.1.2. Basic flow of the algorithm. The basic flow of the state estimation algorithm based on weighted least squares is shown in Fig. 5, and the specific computational steps are as follows:

Step 1: Input the network parameters, measurement data, given the initial values of the state variables and the convergence conditions.

Step 2: Set the number of iterations $k = 1$.

Step 3: Calculate measurements $h(\hat{x}^{(k)})$ as well as Jacobi matrix $H(\hat{x}^{(k)})$ from the existing state variables.

Step 4: Calculate the information matrix $G(\hat{x})$ using the Jacobi matrix $H(\hat{x})$ as well as the measurement weights though descending W.

Step 5: Calculate the corrections to the state variables $\Delta\hat{x}^{(k)}$.

Step 6: Determine whether the convergence condition is satisfied: if $\max\left|\Delta\hat{x}^{(k)}\right| \le \varepsilon$, end the computation, otherwise, $k = k+1$ and make corrections to the state variables and return to step 3 to continue the iteration.

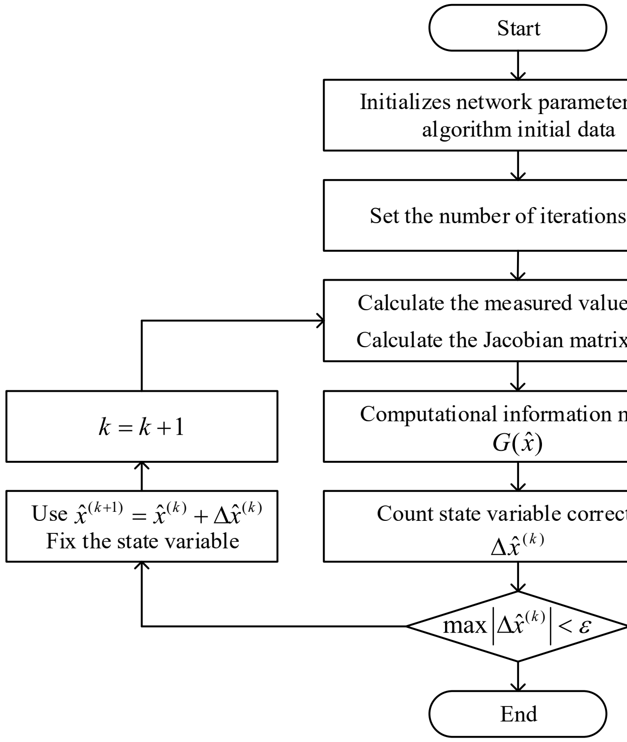

Fig. 5. Basic flow of weighted least squares state estimation algorithm

3.1.3. Handling of Equation Constraints. Currently, the most common approach is to consider the zero-injection measure as an equation of equational constraints on the objective function, and to write all zero-injection measures as $c(x) = 0$. Thus, the weighted least squares state estimation model that takes into account the equational constraints can be expressed as:

$$\begin{gathered} \min J(x) = [z - h(x)]^{\dagger} W [z - h(x)] \\ st.c(x) = 0 \end{gathered} \tag{11}$$

The above model can be solved using the Lagrange multiplier method:

First, the Lagrange multiplier equations are constructed by increasing the Lagrange multiplier phase λ:

$$L(x) = J(x) + \lambda^T c(x) \tag{12}$$

The Lagrangian equations are derived separately for the state variables as well as for the Lagrangian multipliers and the derivatives are made zero:

$$\frac{\partial L}{\partial x} = -2H^T W[z - h(x)] + C^T \lambda = 0 \tag{13}$$

$$\frac{\partial L}{\partial \lambda} = c(x) = 0 \tag{14}$$

Eq. $C = \partial c / \partial x$.

Writing Eqs. (13) and (14) uniformly in matrix form:

$$\begin{bmatrix} 2H^T W H & C^T \\ C & 0 \end{bmatrix} \begin{bmatrix} \Delta x \\ \lambda \end{bmatrix} = \begin{bmatrix} H^T W \Delta z \\ \Delta c \end{bmatrix} \tag{15}$$

The state estimation problem with equation constraints can be solved iteratively using Eq. (15), and this method can ensure that the state estimation result of the injected power at zero-injection nodes is strictly zero. However, this algorithm adds Lagrange multipliers to the state estimation, and due to the large number of zero-injection nodes, the Lagrange multiplier method will DD increase the computational scale and reduce the computational efficiency.

3.2. Distribution Network Hybrid Measurement State Estimation and Monitoring

3.2.1. Measurement transformations. For conventional PQ-type loads, the injected current is derived from the load power measurements as well as the node voltage estimates for each iteration:

$$I_{lri}^{\Lambda f} + jI_{lxi}^{M} = \left(\frac{P_{li} + jQ_{li}}{\tilde{V}_i} \right)^* \tag{16}$$

where P_k, Q_n denotes the node i load active and reactive measurements, respectively, $I_m^M, I_k i^M$ denotes the real and imaginary parts of the node i load equivalent injected current measurement, respectively; $\tilde{v}_i$ is the load node i voltage.

For asynchronous wind turbine and photovoltaic power generation systems, they can be regarded as PQ(V) nodes and PQ nodes, respectively, and their injected currents are calculated similarly to loads:

$$I_{gri}^{M} + jI_{gxi}^{M} = \left(\frac{P_{gi} + jQ_{gi}}{\tilde{V}_i} \right)^* \tag{17}$$

where P_{gi}, Q_{gi} denotes the DG active and reactive power measurements at node i, respectively, $I_{xn}^{''}, I_{gn}^{''}$ denotes the real and imaginary parts of the DG equivalent injected power measurements at node i, respectively; and $\tilde{V}_i$ is the DG node i voltage.

For the branch power measurements, similar to the load and DG injected power measurements, they can be converted to equivalent branch power flow measurements:

$$I_{brj}^{M} + jI_{bxj}^{M} = \left(\frac{P_{brj} + jQ_{brj}}{\tilde{V}_j} \right)^{\bullet} \tag{18}$$

where $P_h rj, Q_h rj$ represents the active and reactive power measurements at the first end of branch j, $I_h rj^M, I_h xj^M$ represents the real and imaginary parts of the equivalent power measurement in branch j, and $\tilde{v}_j$ is the voltage at the first node of branch j where the corresponding branch power measurement is located.

3.2.2. Measurement Functions and Jacobi Matrices:

1) For node injection current phase measurement, the measurement function is:

$$I_n^C + jI_{xi}^C = I_{brm} - \sum_{n \in \Pi_i} I_{brm} + j(I_{bxm} - \sum_{n \in \Pi_i} I_{bxn}) \tag{19}$$

where I_n^c, I_{xi}^c is the calculated value of the real and imaginary parts of the injection current at node i, respectively; I_{brm}, I_{bxm} denotes the real and imaginary parts of the upstream branch current at node i, respectively; Π_i denotes the downstream node of node i; and I_{bm}, I_{hxn} denotes the real and imaginary parts of the downstream branch current at node i, respectively.

For the injection current measurement at node k, the corresponding row of the Jacobi matrix can be expressed as:

$$I_{rk} \to \left[\frac{\partial I_{rk}}{\partial V_{rs}} \frac{\partial I_{rk}}{\partial V_{xs}} \cdots \frac{\partial I_{rk}}{\partial I_{brj}} \frac{\partial I_{rk}}{\partial I_{bzj}} \cdots \right]$$
$$I_{xk} \to \left[\frac{\partial I_{xk}}{\partial V_{rs}} \frac{\partial I_{xk}}{\partial V_{xs}} \cdots \frac{\partial I_{xk}}{\partial I_{brj}} \frac{\partial I_{xk}}{\partial I_{bzj}} \cdots \right] \quad (20)$$

The specific elements are shown below:

$$\frac{\partial I_{rk}}{\partial V_{rs}} = 0 \quad \frac{\partial I_{rk}}{\partial V_{xs}} = 0 \quad (21)$$

$$\frac{\partial I_{xk}}{\partial V_{rs}} = 0 \quad \frac{\partial I_{xk}}{\partial V_{xs}} = 0 \quad (22)$$

$$\frac{\partial I_{xk}}{\partial I_{bxj}} = \begin{cases} 1, & j \text{ is the upstream branch of } k \\ -1, & j \text{ is the downstream branch of } k \\ 0, & j \text{ is not related to } k \end{cases}$$
$$\frac{\partial I_{nk}}{\partial I_{bxj}} = \begin{cases} 1, & j \text{ is the upstream branch of } k \\ -1, & j \text{ is the downstream branch of } k \\ 0, & j \text{ is not related to } k \end{cases} \quad (23)$$

2) For branch current phase measurement, the measurement function is:

$$I_{brj}^C + jI_{bxj}^C = I_{brj} + jI_{bxj} \quad (24)$$

where $I_{brj}^C, I_{b\pi j}^C$ is the calculated value of the real and imaginary parts of the current of branch j, respectively.

For the current measurement of branch k, the corresponding row of the Jacobi matrix can be expressed as:

$$I_{brk} \to \left[\frac{\partial I_{brk}}{\partial V_{rs}} \quad \frac{\partial I_{brk}}{\partial V_{xs}} \quad \cdots \quad \frac{\partial I_{brk}}{\partial I_{brj}} \quad \frac{\partial I_{brk}}{\partial I_{bzj}} \quad \cdots \right]$$
$$I_{bxk} \to \left[\frac{\partial I_{bxk}}{\partial V_{rs}} \quad \frac{\partial I_{bxk}}{\partial V_{xs}} \quad \cdots \quad \frac{\partial I_{bxk}}{\partial I_{bxj}} \quad \frac{\partial I_{bxk}}{\partial I_{bxj}} \quad \cdots \right] \quad (25)$$

The specific elements are shown below:

$$\frac{\partial I_{brk}}{\partial V_{rs}} = 0 \quad \frac{\partial I_{brk}}{\partial V_{rs}} = 0 \quad (26)$$

$$\frac{\partial I_{bxk}}{\partial V_{rs}} = 0 \quad \frac{\partial I_{bxk}}{\partial V_{rs}} = 0 \quad (27)$$

$$\frac{\partial I_{brk}}{\partial I_{brj}} = \begin{cases} 1, & j = k \\ 0, & j \neq k \end{cases}$$
$$\frac{\partial I_{bxk}}{\partial I_{bxj}} = \begin{cases} 1, & j = k \\ 0, & j \neq k \end{cases} \quad (28)$$

3.2.3. Handling of zero-injection nodes. For the zero-injection node, as shown in Fig. 6, since the injected power of node i is strictly zero, its injected current is also zero. Therefore, its upstream branch current is equal to the sum of its downstream branch currents, and the constraint equation for zero-injection node i can be expressed as follows, using the real and imaginary parts of the branch currents as state variables:

$$I_{brn} = I_{br1} + I_{br2} + \ldots + I_{brn} \tag{29}$$

$$I_{bxn} = I_{bx1} + I_{bx2} + \ldots + I_{bxm} \tag{30}$$

where I_{brn} and I_{bxn} denote the real and imaginary parts of the branch current upstream of node i, respectively; I_{brn} and I_{bxm} are the real and imaginary parts of the mth branch current downstream of the node.

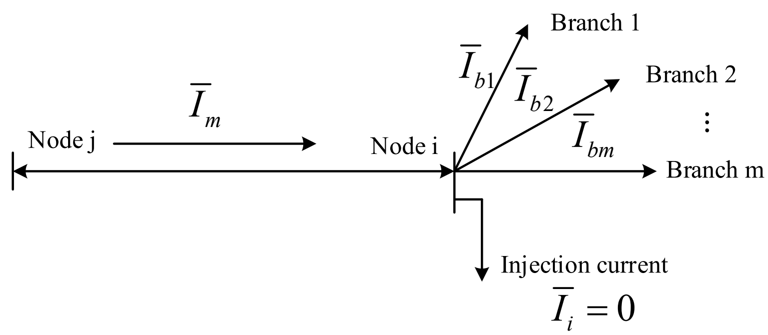

Fig. 6. Zero injection node diagram

3.3. Example analysis

The voltage level of the distribution network used in the example is 12.66 kV and contains a total of 33 nodes and 32 branches. The calculation is carried out by using the scalar value, and the selected voltage base value is the same as the voltage level of the distribution network, which is 12.66 kV, and the power base value is 10 MW, and the maximum allowable error εx is taken as 10-6. Simulation is carried out by using the Matlab R2016a software, and the hardware is the Intel(R) Core(TM) i5-8265U CPU@1.60 GHz. In order to fully validate the the effect of state estimation at the time of PV power access, the following 2 working conditions are illustrated as an example.

3.3.1. Case 1. In the nodes numbered 5, 21, 32 access to the rated power of 20kW PV power generation system, and then based on the above weighted least squares method, the state of the distribution network for PV energy access is estimated. Limited to space, here only selected nodes 1-16 state estimation results as an example to analyze and illustrate; PV access before and after the distribution system in the node voltage specification, the specific value of the phase angle as shown in Table 3, the trend of change as shown in Figure 7.

From the table and figure, PV access before and after the node voltage Mississippi curve almost completely overlap, most of the node voltage Mississippi change very little, the voltage phase angle and the balance of the node of the difference between the node are reduced, of which 14, 15, 16 nodes of the voltage phase angle of the absolute value of the reduction of the larger, which shows that the access of PV to play a role in improving the role of the phase angle of the node voltage.

Table 3. The voltage mark and voltage Angle of the posterior node of the pv

Node number	After pv access		Pv access	
	Voltage mark	Voltage Angle /(°)	Voltage mark	Voltage Angle /(°)
1	1.0543	0.0000	1.0545	0.0000
2	1.0451	-0.5622	1.0447	-0.5642

3	1.0315	-0.4969	1.0315	-0.4984
4	1.0251	-0.4183	1.0252	-0.4218
5	1.0177	-0.3317	1.0176	-0.3376
6	1.0005	-0.3399	1.0005	-0.3466
7	0.9984	-0.5142	0.9984	-0.5193
8	0.9941	-0.489	0.9942	-0.4938
9	0.9895	-0.538	0.9896	-0.5416
10	0.9855	-0.5788	0.9856	-0.5811
11	0.9844	-0.5754	0.9845	-0.5775
12	0.9832	-0.5717	0.9833	-0.5737
13	0.9815	-0.6364	0.9816	-0.6378
14	1.0415	-0.6834	1.0415	-0.6996
15	1.0403	-0.7076	1.0403	-0.7286
16	1.0397	-0.7342	1.0397	-0.7526

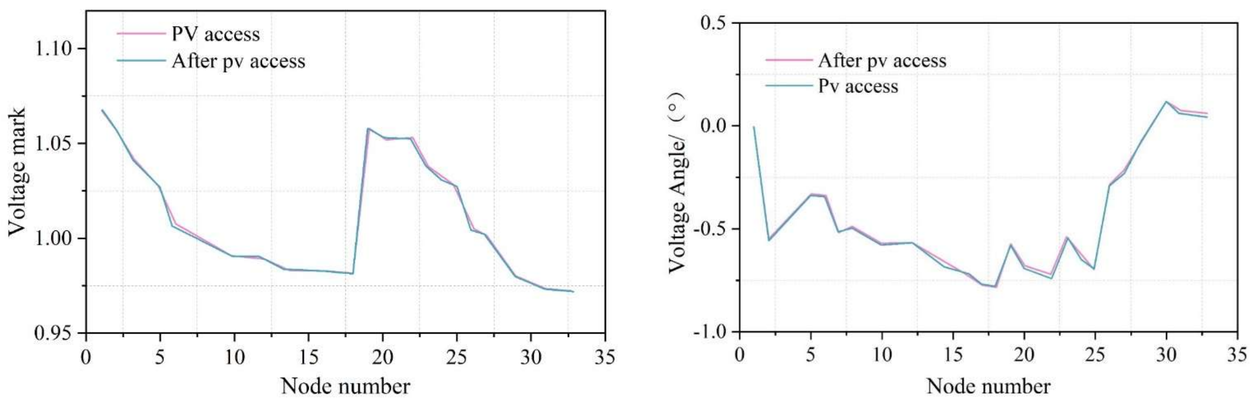

(a) Voltage scale change (b)Voltage Angle variation

Fig. 7. Unv and voltage phase angle change of pv (20 kw) connected to 5,21,32 nodes

3.3.2. Case 2. In order to analyze the change of the system state quantity of the PV system at higher rated output, the 300 kW PV system is still accessed at nodes 5, 21, and 32. State estimation of the PV access before and after the distribution system part of the node voltage value, phase angle trend shown in Figure 8. As can be seen from the figure, in terms of the node voltage Mississippi, with PV access before and PV rated output of 20 kW compared to show some considerable changes: PV access to the node near the Mississippi voltage has a small degree of increase while some nodes of the Mississippi voltage has decreased, the entire system voltage Mississippi shows little fluctuation. For the node voltage phase angle, compared with the PV access before the change is more prominent: PV access to the node near the phase angle of the voltage has increased significantly, while some nodes of the phase angle is a more significant reduction; with the PV rated output of 20kW compared to the fluctuations in the phase angle of the system voltage is more intense.

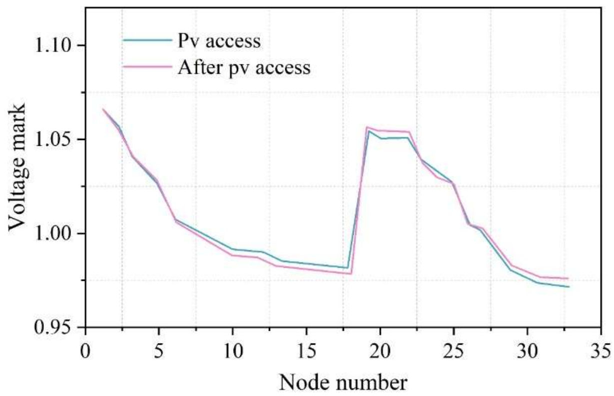

(a) Voltage scale change

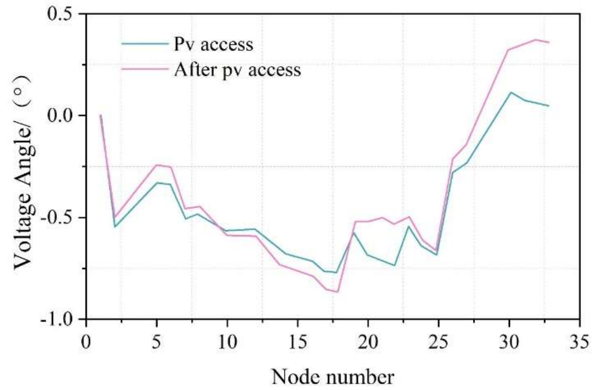

(b) Voltage Angle variation

Fig. 8. Variation of voltage and voltage phase Angle of some nodes

4. Optimization of operation and scheduling of high percentage of DGs connected to the distribution network

4.1. Mathematical model for optimization of high percentage of DG output in distribution network

4.1.1. Optimization objectives. Finally in order to be able to operate the network in a more economical way, the network active network loss should be minimized, i.e:

$$\min F_3(x) = \sum_{(i,j)\in B} g_{ij}(V_i^2 + V_j^2 - 2V_iV_j\cos\theta_{ij}) \tag{31}$$

where B is the set of network branches, i, j is the first and last node number of the branch, θ_{ij} is the phase angle difference of the voltage at node i, j, and $g_i j$ is the branch conductance between nodes i, j.

For the above three objective functions, a weighted approach is used to transform the multi-objective optimization model into a single-objective optimization problem. The specific objective functions are as follows:

$$\min F(x) = -w_1 \cdot F_1(x) / F_1^0 + w_2 \cdot F_2(x) / F_2^0 + w_3 \cdot F_3(x) / F_3^0 \tag{32}$$

where F_1^0, F_2^0, F_3^0 is the initial value of each of the three objective functions before optimization, w_1, w_2, w_3 is the weight of each of the three objective functions and all three are greater than 0. The first term takes a negative sign because the original objective of the first term is to maximize and the objective of the fused function is to minimize, so a negative sign is added.

4.1.2. System constraints. While optimizing the network objective function, the constraints of network operation should be satisfied. Such as trend equation constraints, node voltage magnitude constraints, line power constraints and control quantity constraints.

$$\begin{cases} P_{DG,i} - P_{d,j} - V_i \sum_{j=1}^{n} V_j (G_{ij}\cos\theta_{ij} + B_{ij}\sin\theta_{ij}) = 0 \\ Q_{DG,i} - Q_{d,i} - V_i \sum_{j=1}^{n} V_j (G_{ij}\cos\theta_{ij} - B_{ij}\sin\theta_{ij}) = 0 \end{cases} \tag{33}$$

Eq. (33) is the current equation constraints, $P_D G, l, Q_{DG,l}, P_{d,l}, Q_{d,l}$ is the active and reactive output of the DG connected at node i, and the active and reactive loads, respectively, and G_{i_y}, B_{i_y} is the corresponding element in the node conductivity matrix.

$$P_{DG,i}^{\min} \le P_{DG,i} \le P_{DG,i}^{\max} \tag{34}$$

$$Q_{DG,i}^{\min} \le Q_{DG,i} \le Q_{DG,i}^{\max} \tag{35}$$

$$V_i^{\min} \le V_i \le V_i^{\max} \tag{36}$$

$$\begin{gathered} Sb_k = \sqrt{Pb_k^2 + Qb_k^2} \le \overline{Sb_k} \\ \left|Pb_k\right| = \left|V_i^2 G_{ij} - V_i V_j (G_{ij}\cos\theta_{ij} + B_{ij}\sin\theta_{ij})\right| \\ \left|Qb_k\right| = \left|V_i^2 B_{ij} + V_i V_j (G_{ij}\sin\theta_{ij} - B_{ij}\cos\theta_{ij})\right| \end{gathered} \tag{37}$$

Eq. (34) is the maximum and minimum constraints on the control variables; Eq. (36) is the upper and lower constraints on the voltage amplitude at each node of the network; Eq. (37) is the power constraint of the branch, Sb_k is the apparent power of branch k, Pb_k, Qb_k is the active and reactive power flowing through branch k, and $\overline{Sb_k}$ is the upper limit of the apparent power of branch k.

4.2. Optimizing the model solving algorithm

4.2.1. Simplification of the optimization model. The combined objective function and constraints can be used to abbreviate the original optimization problem into the following constrained optimization problem form:

$$\begin{aligned} \min \quad & f(u,x) \\ s.t. \quad & h(u,x) = \theta \\ & g(x) \le \theta \\ & \underline{u} \le u \le \overline{u} \end{aligned} \tag{38}$$

where u is the network independent control quantity, which in this paper refers to the active reactive power output of DG; x is the voltage state quantity of each node. The equations in Eq. are constrained to be the current equations. Although state quantity x cannot be expressed analytically in terms of control quantity u, it can be solved by the tidal equation when u is determined x. Therefore, the tidal equation $h(x,u) = 0$ contains a function of state quantity x with respect to u, denoted $F(u) = f(u,x), G(u) = g(x)$, and then the constrained optimization problem (38) can also be written in the following form:

$$\begin{aligned} \min \quad & F(u) \\ s.t. \quad & G(u) \le 0 \\ & \underline{u} \le u \le \overline{u} \end{aligned} \tag{39}$$

4.2.2. Solution algorithm based on the quadratic programming method for trust domain sequences. The two rows are the number of equation constraints and the number of inequality constraints, respectively. Considering that the system of first-order equations for the actual trend equation always has a solution, the θ-variable removal can be simplified to the following form:

$$\begin{aligned} \min \quad & \frac{1}{2} d^T B_k d + \nabla f_k^T d + \sigma_k \times \delta \\ s.t. \quad & \nabla h_k^T d + h_k = 0 \\ & \nabla g_k^T d + g_k \le \delta \times e_g \\ & \|d\|_\infty \le \Delta_k, \delta \ge 0 \end{aligned} \tag{40}$$

After solving problem (40) to obtain the optimal step size d, it is necessary to make a judgment on the step size and the current radius of the trust domain. The second-order Taylor expansion $\Phi(d)$ of the original objective function is defined here as:

Using the trust domain sequential quadratic programming method, for the constrained optimization problem, referring to Eq. (40), the subproblem of the k rd iteration is:

$$\begin{aligned} \min \quad & C_k d + \frac{1}{2} d^T B_k d + \sigma_k \cdot \delta \\ s.t. \quad & A_k d \le -G_k + \delta \cdot e_g \\ & \underline{u} - u_k \le d \le \overline{u} - u_k \\ & \| d \|_\infty \le \Delta_k \\ & \delta \ge 0 \end{aligned} \tag{41}$$

where $C_k = \nabla_u F(u_k), A_k = \nabla_u G(u_k), B_k$ is the objective function Hessian matrix, G_k is the value of function $G(u)$ at the k th iteration point, σ_k is the penalty function, $\delta = \| (A_k^T d + G_k)^+ \|_\infty$

The expression of matrix C_k, A_k, B_k is as follows:

$$\begin{aligned} C_k &= \frac{\partial F}{\partial u} = \frac{\partial f}{\partial x} \times \frac{\partial x}{\partial u} + \frac{\partial f}{\partial u} \Big|_{u=u_k, x=x_k} \\ A_k &= \frac{\partial G}{\partial u} = \frac{\partial g}{\partial x} \times \frac{\partial x}{\partial u} \Big|_{u=u_k, x=x_k} \\ B_k &= \frac{\partial^2 f}{\partial u^2} + (\frac{\partial x}{\partial u})^T \times \frac{\partial^2 f}{\partial x^2} \times \frac{\partial x}{\partial u} \end{aligned} \tag{42}$$

Solve x_k from the control variable u_k at the k st iteration through the tidal equation $h(x,u) = 0$. Take a partial derivative of the tidal equation:

$$\frac{\partial h}{\partial u} + \frac{\partial h}{\partial x} \times \frac{\partial x}{\partial u} = 0 \tag{43}$$

$\frac{\partial h}{\partial x}$ is the Jacobi matrix of the tidal equation, which is obtained from (43):

$$\frac{\partial x}{\partial u} = -(\frac{\partial h}{\partial x})^{-1} \frac{\partial h}{\partial u} \tag{44}$$

The bias matrices in (42), (43) and (44) above are all sparse matrices, and the calculation of Eq. (44) can be regarded as the solution of a series of linear equations whose coefficient matrices are the Jacobi matrices of the tidal equations, and there is no need to form the factorization table of the coefficient matrices again, and it is necessary to follow the factorization table of the Jacobi matrices in the tidal calculations for the calculations. By fixing the Jacobi matrices of the tidal equations in a certain way of approximation, the factor tables need to be formed only once, and the calculation of the tidal currents as well as the calculation of the partial derivatives will be greatly simplified. The control variable u has a very low dimension, so the above three equations are not very computationally intensive.

4.2.3. Effective set methods for solving subquadratic programming problems. The basic idea of the effective set method is to start from an initial point, consider a set of certain positive constraints, solve its corresponding quadratic programming subproblem containing only equation constraints after determining the effective set, and judge whether the solution of the subproblem is the optimal solution of the original quadratic programming problem according to the nonnegativity of the Lagrange multiplier vectors of the subproblem, and the solution is the optimal solution if all the multiplicities of the corresponding inequality are nonnegative, and the solution is the optimal solution if all the multiplicities are nonnegative, and the solution is the optimal solution if all the multiplicities are nonnegative. If all the multipliers of the corresponding inequality are non-negative, then it is the optimal solution, otherwise, we need to adjust the valid set again, and iterate gradually until we get the optimal solution.

For the quadratic programming problem like (41), it is abbreviated as follows:

$$\begin{aligned} \min \quad & \frac{1}{2}x^T Bx + c^T x \\ s.t. \quad & A_{in}x \le b_{in} \end{aligned} \tag{45}$$

4.2.4. Solving Distributed Power Optimization Flowchart. The steps to solve the distributed power supply optimization problem by using the quadratic programming method of trust domain sequence are described as follows:

1) Set the initial value of each control quantity u_0; set the maximum trust domain radius $\overline{\Delta} = 0.5 \times \| \overline{u} - \underline{u} \|_\infty$ ($\overline{u}, \underline{u}$ for the upper and lower bounds of the control variables, respectively) of variable u in the optimization problem, and the initial trust domain radius $\Delta_0 = 0.5 \times \overline{\Delta}$; set the solution accuracy ε_1, constraint accuracy ε_2, the initial penalty parameter σ_0, and the maximum penalty parameter $\overline{\sigma}$ of the control variables. Set $k = 0$.

2) Solve the tidal equations based on the current control variable values to obtain the values of state quantities such as voltage nodes and branch power;

3) Form the sub-problem and solve it, and the solution method adopts the effective set method. Obtain the optimal step d and update $u_{k+1} = u_k + d$;

4) According to the current value of control variables u_{k+1} to calculate the trend to get the network voltage and branch current and other state quantities of information. If $\| G_k + 1^+ \|_\infty < \varepsilon_2$ each constraint of the network is satisfied and $\| d \| < \min(\varepsilon_1, \Delta_k)$ is satisfied, the calculation is terminated, the calculation results are output, and go to step 5;

5) If $r_k < 0.25$, reject the current step, set $u_t + 1 := u_{t+1} - d, \Delta_{k+1} = \| d \|_\infty / 2$, and turn to step 2) If $r_k \ge 0.25$, accept the step, and adjust the trust domain and penalty parameters and turn to step 3).

4.3. Example Simulation

Taking the three moments of 6 o'clock, 17 o'clock and 21 o'clock, the voltage profile and the three moments of reactive power source reactive output profile are shown in Fig. 9 to Fig. 10 respectively.

As can be seen from Fig. 9, 6:00 a.m. moment belongs to just to come to the morning peak, so its load increases but not to the peak moment is large, so 6:00 a.m. moment voltage value is higher, but there are still some nodes voltage has over the limit, in the reactive power control zoning cooperative control strategy, the nodes voltage has a more obvious rise, the node voltage has a good improvement of many voltages have been elevated to More than 1 pu greatly increased the stability of the system. At the moment of 17 o'clock near night, because the load of each part of this time began to increase, so the system voltage of each node has a more drastic decline, more node voltage fell below the permissible range or even down to 0.90pu, and the imbalance of the voltage within the system is further aggravated.

As can be seen from Fig. 10, after joining the reactive power control zonal cooperative control strategy, the voltage at each node still has a more obvious rise, and the voltage rise situation through the cooperative control strategy still has some voltages exceeding 1 pu. At 21:00, the load situation in each region at this time reaches the maximum, which belongs to the evening peak peak of the electricity consumption. The poor voltage quality is further aggravated, and more nodes' voltages drop below the permissible range, and the voltage imbalance in the system becomes more serious. With the activation of the cooperative control strategy of local reactive power control zones, compared with the system at 6:00 p.m. and 17:00 p.m., although the voltage of many nodes is on the low side compared with the previous one, and even the voltage of individual nodes has dropped to the lower limit, and there is a risk of overrun, but the voltage increase of each area after the cooperative control strategy of reactive power control is still more than 1pu. However, the reactive power control zonal cooperative control strategy still stabilizes the system's node voltages within the appropriate voltage deviation range. According to the above three moments of voltage and reactive power output, the reactive power control zonal cooperative control strategy can control the voltage within the appropriate range when the voltage is reduced, and the output of each reactive power source has not reached the upper limit, so it can be seen that in the face of more serious voltage drop, the reactive power control zonal cooperative control strategy can still control the voltage within the appropriate range.

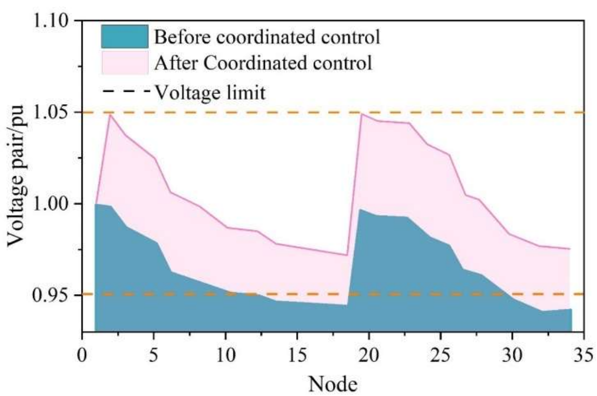

(a)The voltage of six times

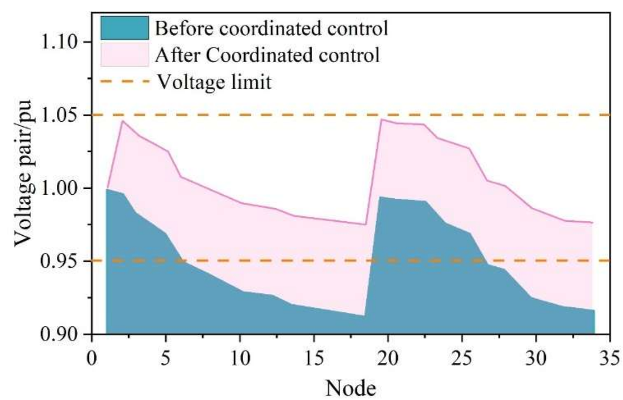

(b)17 moment voltage

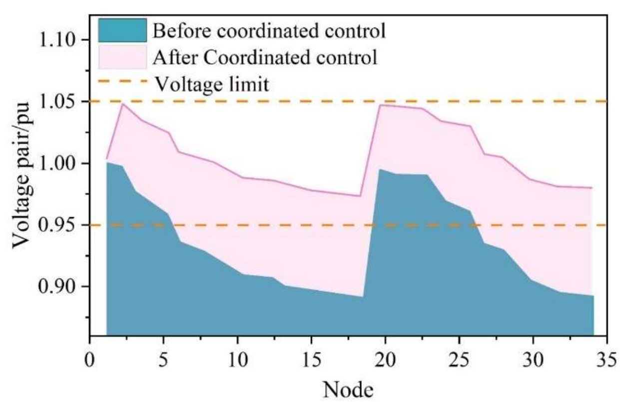

(c)The voltage of the 21 moment

Fig. 9. Voltage situation plot at three moments

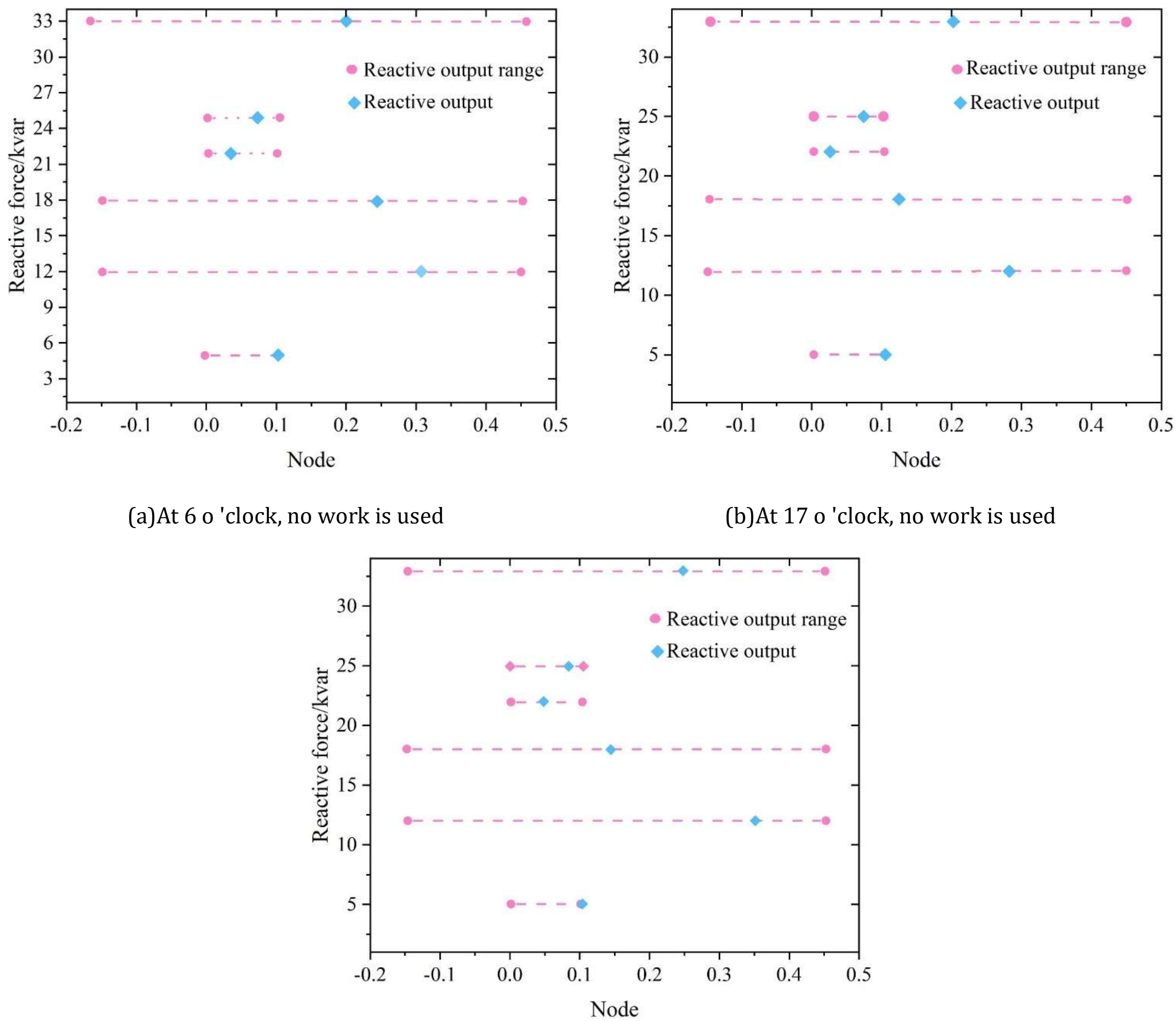

(a)At 6 o 'clock, no work is used

(b)At 17 o 'clock, no work is used

(c)The force of no work is done at 21

Fig. 10. Reactive power source reactive power output curve of three moments

5. Conclusion

In this paper, by analyzing the impact of high proportion distributed DG access on distribution network, then using machine learning algorithms for estimation and detection of distribution network state, and finally optimization of adjustable characteristics, the conclusions are obtained as follows:

1) Distributed power access point has the role of supporting voltage but the static voltage index of access power is high and the operation is unstable. The system network loss with the change of access capacity shows a trend of first decreasing and then increasing, and the minimum value of the total network loss of the simulated system is 15% of the total network loss of the system when there is no distributed power supply access.

2) Under the condition that the node number accessed by the PV remains unchanged. When the rated output of the PV is not large on the system nodes of the voltage Mississippi and phase angle will not have a significant impact, but with the increase in the rated output of the PV will make the system voltage amplitude and phase angle fluctuations are increasingly large, the overall rated output of the different PV on the phase angle of the system voltage have a corresponding degree of improvement, but in some cases will also make some nodes of the phase angle of the voltage and the balance of the

nodes of the deviation becomes very large. However, under certain circumstances, the phase angle of certain node voltages will also deviate from that of the equilibrium node.

3) A multi-objective reactive power optimization model is established by taking the network loss, voltage deviation, and economic index of equipment regulation as the optimization objectives, and taking the current, node voltage, and energy storage as the constraints, as well as the number of shunt capacitor bank switching and the reactive power output of distributed power sources as the decision variables. The simulation results show that the zonal cooperative control strategy can effectively improve the voltage level and reduce the network loss in the distribution network area and improve the stability of the system.

Funding

Research and demonstration of multi-time scale adaptive whole-area distribution network self-healing technology considering distributed resource carrying capacity - Topic 3: Research on the Carrying Capacity of Distribution Networks for Distributed Resources and Optimization Control Technologies (GZKJXM20222431).

References

[1] Li, S., & Li, J. (2017). Condition monitoring and diagnosis of power equipment: review and prospective. High Voltage, 2(2), 82-91.

[2] Malhotra, R., Alzahawi, T., & McLeod, E. (2019, May). Management and maintenance of electrical equipment in industrial facilities. In 2019 IEEE/IAS 55th Industrial and Commercial Power Systems Technical Conference (I&CPS) (pp. 1-6). IEEE.

[3] Betti, A., Crisostomi, E., Paolinelli, G., Piazzi, A., Ruffini, F., & Tucci, M. (2021). Condition monitoring and predictive maintenance methodologies for hydropower plants equipment. Renewable Energy, 171, 246-253.

[4] Fei, G., Pengfei, J., Jiayun, Z., Ning, Y., Wentong, S., & Sizhuo, L. (2023, December). Research on Decision Method for Power Equipment Conditional Maintenance Strategy Based on Markov Process. In 2023 7th International Conference on Power and Energy Engineering (ICPEE) (pp. 194-199). IEEE.

[5] Babak, V. P., Babak, S. V., Eremenko, V. S., Kuts, Y. V., Myslovych, M. V., Scherbak, L. M., ... & Zaporozhets, A. O. (2021). Models and measures for the diagnosis of electric power equipment. Models and Measures in Measurements and Monitoring, 99-126.

[6] Long, L. (2022). Research on status information monitoring of power equipment based on Internet of Things. Energy Reports, 8, 281-286.

[7] Zhou, H., Pan, P., & Yu, J. (2019, April). Condition monitoring and fault diagnosis of power equipment. In IOP Conference Series: Earth and Environmental Science (Vol. 252, No. 3, p. 032078). IOP Publishing.

[8] Zhao, J., & Yue, X. (2020). Condition monitoring of power transmission and transformation equipment based on industrial internet of things technology. Computer Communications, 157, 204-212.

[9] Luo, J., Huang, J., & Li, H. (2021). A case study of conditional deep convolutional generative adversarial networks in machine fault diagnosis. Journal of Intelligent Manufacturing, 32(2), 407-425.

[10] Wang, B., Baraldi, P., & Zio, E. (2022). Deep multiadversarial conditional domain adaptation networks for fault diagnostics of industrial equipment. IEEE Transactions on Industrial Informatics, 19(8), 8841-8851.

[11] Contreras-Valdes, A., Amezquita-Sanchez, J. P., Granados-Lieberman, D., & Valtierra-Rodriguez, M. (2020). Predictive data mining techniques for fault diagnosis of electric equipment: A review. Applied Sciences, 10(3), 950.

[12] Ullah, I., Yang, F., Khan, R., Liu, L., Yang, H., Gao, B., & Sun, K. (2017). Predictive maintenance of power substation equipment by infrared thermography using a machine-learning approach. Energies, 10(12), 1987.

[13] Nsaif, Y. M., Lipu, M. H., Ayob, A., Yusof, Y., & Hussain, A. (2021). Fault detection and protection schemes for distributed generation integrated to distribution network: Challenges and suggestions. IEEE Access, 9, 142693-142717.

[14] Zhuang, T., Ren, M., Gao, X., Dong, M., Huang, W., & Zhang, C. (2019). Insulation condition monitoring in distribution power grid via IoT-based sensing network. IEEE Transactions on Power Delivery, 34(4), 1706-1714.

[15] Massaro, A., Galiano, A., Meuli, G., & Massari, S. F. (2018). Overview and application of enabling technologies oriented on energy routing monitoring, on network installation and on predictive maintenance. International Journal of Artificial Intelligence and Applications (IJAIA), 9(2).

[16] Alsheryani, R. M., Alkaabi, S. S., Alkaabi, S. S., Aldhaheri, A. M., Khouri, F. I., Alharmoodi, S. I., ... & Alhajeri, A. S. (2019, November). Applying artificial intelligence (AI) for predictive maintenance of power distribution networks: A case study of al ain distribution company. In 2019 International Conference on Electrical and Computing Technologies and Applications (ICECTA) (pp. 1-5). IEEE.

[17] Menke, J. H., Bornhorst, N., & Braun, M. (2019). Distribution system monitoring for smart power grids with distributed generation using artificial neural networks. International Journal of Electrical Power & Energy Systems, 113, 472-480.

[18] Payne, E. K., Lu, S., Wang, Q., & Wu, L. (2019). Concept of designing thermal condition monitoring system with ZigBee/GSM communication link for distributed energy resources network in rural and remote applications. Processes, 7(6), 383.

[19] Mahmoud, M. A., Md Nasir, N. R., Gurunathan, M., Raj, P., & Mostafa, S. A. (2021). The current state of the art in research on predictive maintenance in smart grid distribution network: Fault's types, causes, and prediction methods—A systematic review. Energies, 14(16), 5078.

[20] Vita, V., Fotis, G., Chobanov, V., Pavlatos, C., & Mladenov, V. (2023). Predictive maintenance for distribution system operators in increasing transformers' reliability. Electronics, 12(6), 1356.

[21] Li, K., Xie, Z., Zeng, D., Li, W., Luo, J., Wang, M., ... & Xia, C. (2021). Power cable vibration monitoring based on wireless distributed sensor network. Procedia Computer Science, 183, 401-411.

[22] Heidari, S., Fotuhi-Firuzabad, M., & Lehtonen, M. (2017). Planning to equip the power distribution networks with automation system. IEEE Transactions on Power Systems, 32(5), 3451-3460.

[23] Singh, R. R., Bhatti, G., & Saravanan, D. (2022). New-age condition monitoring of on-load tap changing transformers in distributed energy systems for Industry 4.0. e-Prime-Advances in Electrical Engineering, Electronics and Energy, 2, 100087.

[24] Tang, B. H., & Zhou, Z. X. (2018, May). The design of communication network optical fiber cable condition monitoring system based on distributed optical fiber sensor. In 2018 International Conference on Electronics Technology (ICET) (pp. 97-101). IEEE.

[25] Shuqin Sun,Zhenghai Yuan,Weiqiang Liang,Xin Qi & Guanghao Zhou. (2024). Sensitivity Analysis and Distribution Factor Calculation under Power Network Branch Power Flow Exceedance. Energies(17),4374-4374.

[26] Swati Arora,Mohammad Aljaidi,Mamatha Sandhu,Samar Hussni Anbarkhan & Reetu Malhotra. (2024). Determination of yearly energy savings by CVR in combination with photovoltaic inverter control functions in distribution network. Energy Reports5507-5520.

[27] Y Geng,T Kitahora,S Iio,Y D Choi & M Inagaki. (2024). Study on the optimum design of cross flow water turbines using RSM with weighted least squares method. Journal of Physics: Conference Series(1).